New Journal of Physics
The open access journal for physics

Optomechanical circuits for nanomechanical continuous variable quantum state processing

Michael Schmidt[1,3], **Max Ludwig**[1] **and Florian Marquardt**[1,2]

[1] Friedrich-Alexander-Universität Erlangen-Nürnberg, Staudtstraße 7, D-91058 Erlangen, Germany

[2] Max Planck Institute for the Science of Light, Günther-Scharowsky-Straße 1/Bau 24, D-91058 Erlangen, Germany

E-mail: michael.schmidt@physik.uni-erlangen.de

New Journal of Physics **14** (2012) 125005 (12pp)
Received 4 July 2012
Published 10 December 2012
Online at http://www.njp.org/
doi:10.1088/1367-2630/14/12/125005

Abstract. We propose and analyze a nanomechanical architecture where light is used to perform linear quantum operations on a set of many vibrational modes. Suitable amplitude modulation of a single laser beam is shown to generate squeezing, entanglement and state transfer between modes that are selected according to their mechanical oscillation frequency. Current optomechanical devices based on photonic crystals, as well as other systems with sufficient control over multiple mechanical modes, may provide a platform for realizing this scheme.

[3] Author to whom any correspondence should be addressed.

Contents

1. Introduction

The field of cavity optomechanics studies the interaction between light and mechanical motion, with promising prospects in fundamental tests of quantum physics, ultrasensitive detection and applications in quantum information processing (see [1–3] for reviews). One particularly promising platform consists of 'optomechanical crystals', in which strongly localized optical and vibrational modes are implemented in a photonic crystal structure [4]. So far, several interesting possibilities have been pointed out that would make use of multi-mode setups designed on this basis. For example, suitably engineered setups may coherently convert phonons to photons [5], and collective nonlinear dynamics might be observed in optomechanical arrays [6]. Moreover, optomechanical systems, in general, have been demonstrated to furnish the basic ingredients for writing quantum information from the light field into the long-lived mechanical modes [7–9]. The recent success in ground state laser cooling [10, 11] has opened the door to coherent quantum dynamics in optomechanical systems.

In this paper, we propose a general scheme for continuous-variable quantum state processing [12] utilizing the vibrational modes of such structures. We show how entanglement and state-transfer operations can be applied selectively to pairs of modes, by suitable intensity modulation of a single incoming laser beam. We discuss limitations for entanglement generation and transfer fidelity, and show how to pick suitable designs to address these challenges.

2. The model

We will first restrict our attention to a single optical mode coupled to many mechanical modes, such that the following standard optomechanical Hamiltonian describes the photon field $\hat{a}$, the phonons $\hat{b}_l$ of different localized vibrational modes ($l = 1, 2, \ldots, N$), their mutual coupling and the laser drive:

$$\hat{H} = -\hbar\Delta\hat{a}^\dagger\hat{a} + \sum_l \hbar\Omega_l\hat{b}_l^\dagger\hat{b}_l - \hbar\hat{a}^\dagger\hat{a}\sum_l g_0^{(l)}(\hat{b}_l^\dagger + \hat{b}_l) + \hbar\alpha_L(\hat{a} + \hat{a}^\dagger) + \cdots . \quad (1)$$

We are working in a frame rotating at the laser frequency ω_L with detuning $\Delta = \omega_\mathrm{L} - \omega_\mathrm{cav}$. Here, α_L denotes the coupling to the drive, which is proportional to the laser amplitude. We omitted to

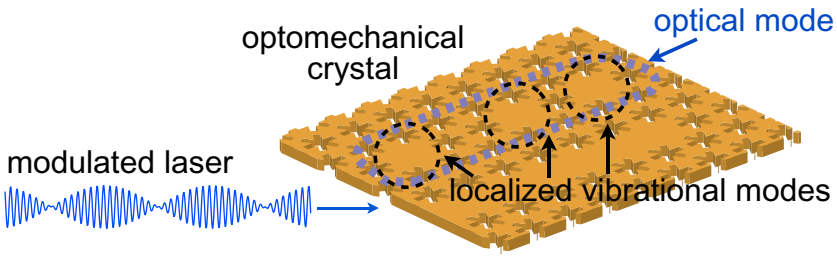

Figure 1. Schematic diagram illustrating an optomechanical crystal with localized vibrational modes, coupled by a common optical mode. The optical mode is driven by an amplitude-modulated laser beam to engineer frequency-selective entanglement, squeezing and state-transfer operations of vibrations (see the main text).

explicitly write down the coupling to the photon and phonon baths, with damping rates κ and Γ_l, respectively, although these will be included in our treatment. The bare (single-photon) coupling constants $g_0^{(l)}$ depend on the overlap between the optical and mechanical mode functions and are of the order of $\omega_{\rm cav} x_{\rm ZPF}/L$, where $x_{\rm ZPF} = (\hbar/2m_l\Omega_l)^{1/2}$ is the mechanical zero-point amplitude. In photonic crystals the effective cavity length L reaches down to wavelength dimensions (see figure 1 for the illustration of a setup).

After the application of the standard procedure of splitting off the coherent optical amplitude induced by the laser, $\hat{a} = \alpha + \delta\hat{a}$, and omitting terms quadratic in $\delta\hat{a}$ (valid for strong drive) to the Hamiltonian, we recover the linearized optomechanical coupling,

$$\hat{H}_{\rm int} = -\hbar(\delta\hat{a} + \delta\hat{a}^\dagger)\sum_l g_l(\hat{b}_l^\dagger + \hat{b}_l) = -\hbar(\delta\hat{a} + \delta\hat{a}^\dagger)\hat{Y}. \tag{2}$$

Here the dressed couplings $g_l = g_0^{(l)}\alpha$ can be tuned via the laser intensity, i.e. the circulating photon number: $|\alpha| = \sqrt{\bar{n}_{\rm phot}}$ ($\alpha \in \mathbb{R}$ without loss of generality). We can now eliminate the driven cavity field (noting that $\delta\hat{a}$ is in the ground state) by second-order perturbation theory: at large detuning $|\Delta| \gg \Omega_l$ the energy scales for phonons and photons separate, and we retain a fully coherent, light-induced mechanical coupling between all the vibrational modes,

$$\hat{H}_{\rm int}^{\rm eff} = \hbar\frac{\hat{Y}^2}{\Delta} = 2\hbar\sum_{l,k} J_{lk}(t)\hat{X}_l\hat{X}_k, \tag{3}$$

where $\hat{X}_l \equiv \hat{b}_l + \hat{b}_l^\dagger$ is the mechanical displacement in units of $x_{\rm ZPF}$. For this to be valid, we have to fulfill $\kappa \ll |\Delta|$, which prevents unwanted transitions. Equation (3) may be viewed as a 'collective optical spring' effect, coupling all the mechanical displacements. The couplings $J_{lk}(t) = g_l g_k/2\Delta$ can be changed *in situ* and in a time-dependent manner via the laser intensity or the detuning. In the numerical simulations, we take $g_0^{(l)} = g_0 x_{\rm zpf}^{(l)}/x_{\rm zpf}^{(1)} = g_0\sqrt{\Omega_1/\Omega_l}$ and assume all modes to have equal masses. This feature will be crucial for our approach described below. Note that if multiple optical modes are driven, the corresponding coupling constants will add.

In general, the couplings in equation (3) will induce quantum state transfer between mutually resonant mechanical modes and entanglement at low temperatures (usually with the help of optomechanical laser cooling). The generation of entanglement between two mechanical

modes based on the bilinear interaction, equation (3), has been analyzed in [13–19] or in [19–22] for entanglement between the light field and the phononic mode. However, these schemes are not easily scalable to many mechanical modes, mainly because it is not possible to address the modes that are to be entangled. Moreover, these schemes produce an entangled steady state that is sensitive to thermal fluctuations. We will describe a different scheme that allows mode-selective entanglement and is particularly suited for multi-mode setups. Its robustness against thermal influence is enhanced, since it employs parametric instabilities for entanglement generation.

3. General scheme

In contrast to the schemes mentioned above, we have in mind a multi-mode situation for continuous variable quantum information processing and are interested in an efficient approach to selectively couple arbitrary pairs of modes, both for entanglement and for state transfer. There are several desiderata to address for a suitable optomechanical architecture of that style: one should be able to (i) switch couplings in time, (ii) easily select pairs for operations, (iii) get by with only one laser (or a limited number), (iv) achieve large enough operation speeds to beat decoherence and (v) scale to a reasonably large number of modes.

3.1. Frequency-selective operations

Static couplings as in equation (3) could be used for selective pair-wise operations if one were able to shift locally the mechanical frequency to bring the two respective modes into resonance. In principle, this is achievable via the optical spring effect, but would require local addressing with independent laser beams. This could prove challenging in a micron-scale photonic crystal, severely hampering scalability.

Instead, we propose to employ frequency-selective operations, by modulating the laser intensity (and thus J) in time. Entanglement generation by parametric driving has recently been analyzed in various contexts, including superconducting circuits [23], trapped ions [24], general studies of entanglement in harmonic oscillators [25–27], optomechanical state transfer and entanglement between the motion of a trapped atom and a mechanical oscillator [28] and entanglement between mechanical and radiation modes [29]. Parametric driving can also lead to mechanical squeezing in optomechanical systems [30].

Let us now consider two modes with coupling $2\hbar J(t)(\hat{X}_1+\hat{X}_2)^2$. Note that for the purposes of our discussion we set $J_{lk}=J$ for the sake of simplicity. The results mentioned below, however, remain valid for the general case of unequal couplings, which is also used for the numerical simulations. The time-dependent coupling is achieved by modulating the laser intensity at a frequency ω of the order of the mechanical frequencies. For $\omega \ll |\Delta|$ the circulating photon number follows adiabatically $|\alpha(t)|^2=|\alpha_{\max}|^2\cos^2(\omega t)$, and we have $J(t)=J\cos^2(\omega t)=J[1+\cos(2\omega t)]/2$. The resulting time-dependent light-induced mechanical coupling can be broken down into several contributions, whose relative importance will be determined by the drive frequency ω. The static terms, $\hbar J(\hat{X}_1+\hat{X}_2)^2$, shift the oscillator frequencies by $\delta\Omega_j=2J$, and give rise to an off-resonant coupling that is ineffective for $|\Omega_1-\Omega_2|\gg J$, but gains influence for $|\Omega_1-\Omega_2|\lesssim J$. In a realistic setup this $\hat{X}_1\hat{X}_2$ interaction might be enhanced due to intrinsically present phonon tunneling between distinct vibrational modes, which could easily be included in the analysis, since it is of the same structure.

Moreover, the static terms contain single mode squeezing terms $\hat{b}_l^\dagger \hat{b}_l^\dagger + \hat{b}_l \hat{b}_l$ that are always off-resonant and of negligible influence. For the oscillating terms

$$\hbar J(\mathrm{e}^{2\mathrm{i}\omega t} + \mathrm{e}^{-2\mathrm{i}\omega t})(\hat{b}_1 + \hat{b}_1^\dagger)(\hat{b}_2 + \hat{b}_2^\dagger), \tag{4}$$

there are three important cases. A mechanical beam-splitter (state-transfer) interaction is selected for a laser drive modulation frequency $\omega = (\Omega_1 - \Omega_2)/2$. In the interaction picture with respect to Ω_1 and Ω_2, the resonant part of the full Hamiltonian reads

$$\hat{H}_{\mathrm{b.s.}} = \hbar J(\hat{b}_2^\dagger \hat{b}_1 + \hat{b}_1^\dagger \hat{b}_2).$$

In contrast, for $\omega = (\Omega_1 + \Omega_2)/2$, we obtain from equation (4) a two-mode squeezing (non-degenerate parametric amplifier) Hamiltonian,

$$\hat{H}_{\mathrm{ent}} = \hbar J(\hat{b}_1 \hat{b}_2 + \hat{b}_1^\dagger \hat{b}_2^\dagger),$$

which can lead to efficient entanglement between the modes. Finally, $\omega = \Omega_j$ selects the squeezing interaction for a given mode,

$$\hat{H}_{\mathrm{sq}} = \hbar(J/2)(\hat{b}_j^2 + \hat{b}_j^{\dagger 2}),$$

out of the full Hamiltonian. These laser-tunable, frequency-selective mechanical interactions are the basic ingredients for the architecture we will develop and analyze here. Furthermore, combinations of these Hamiltonians can be constructed when the laser intensity is modulated with multiple frequencies. Note that one has to keep in mind that the modulation also generates a time-dependent radiation pressure force, $\hbar g_0 |\alpha_{\max}|^2 \cos^2(\omega t)/x_{\mathrm{ZPF}}$, which leads to a coherent driving of each of the mechanical modes for $\omega \approx \Omega_l/2$. For the parameters we choose here, these processes are off-resonant, however.

3.2. Limitations

We now address the constraining factors for the operation fidelity, both for the two-mode and the multi-mode case. At higher drive powers (as needed for fast operations), the frequency–time uncertainty implies that the different processes need not be resonant exactly, with an allowable spread $|\delta\omega| \lesssim J$. The parametric instabilities occur for $|\omega - (\Omega_i + \Omega_j)/2| < J$. Once these intervals start to overlap, process selectivity is lost and the fidelity suffers. At low operation speeds, quantum dissipation and thermal fluctuations will limit the fidelity. This is the essential problem faced by a multi-mode setup, and we will discuss possible remedies further below. The schematic situation for the example of three modes is illustrated in figure 2.

In order to analyze decoherence and dissipation, we employ a Lindblad master equation to evolve the joint state of the mechanical modes. The evolution of any expectation value can be derived from the master equation and is governed by

$$\frac{\mathrm{d}}{\mathrm{d}t}\langle \hat{A} \rangle = \frac{1}{\mathrm{i}\hbar}\langle [\hat{A}, \hat{H}] \rangle + \sum_j (\bar{n}_j + 1)\Gamma_j \langle \mathcal{R}[\hat{b}_j^\dagger]\hat{A} \rangle + \sum_j \bar{n}_j \Gamma_j \langle \mathcal{R}[\hat{b}_j]\hat{A} \rangle.$$

Here $\hat{H}$ describes the vibrational modes and already contains the effective interaction (3), with modulated time-dependent couplings. Γ_j are the damping rates of the vibrational modes, and $\bar{n}_j$ their equilibrium occupations at the bulk temperature. Note that we effectively added the light-induced decoherence rate $\Gamma_{\mathrm{opt}}^{\varphi} \approx g_0^2 \alpha^2 \kappa/\Delta^2 = 2J(\kappa/\Delta)$ to the intrinsic rate $\Gamma\bar{n}$ [31]. $\Gamma_{\mathrm{opt}}^{\varphi}$

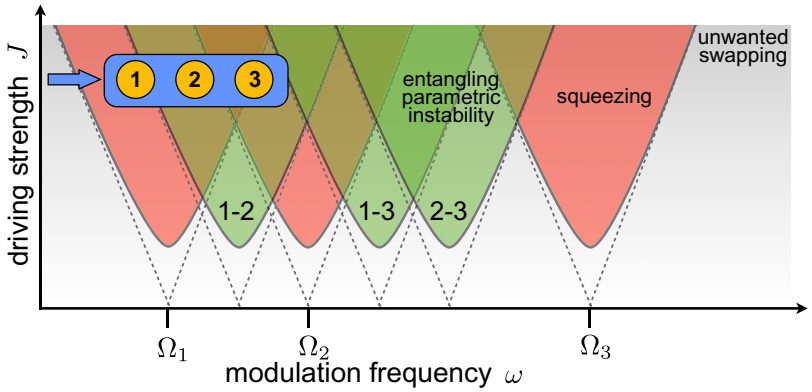

Figure 2. Schematic diagram of the resonance regions for squeezing and entanglement operations between vibrational modes (Ω_1, Ω_2 and Ω_3), induced by harmonically modulating the laser intensity at frequency ω. For too weak laser intensity (small J), dissipation prevents parametric resonances (dashed lines indicate resonance regions without dissipation). With increasing light-induced coupling J dissipation is overcome and regions of parametric resonance for entangling and squeezing operations emerge. By adjusting the modulation frequency ω, these operations can be addressed selectively. When J is further increased, different regions start to overlap and selectivity is lost. At large J unwanted swapping processes occur, leading to an off-resonant coupling between the modes.

is suppressed by a factor $\kappa/|\Delta|$ and can be arbitrarily small for larger detuning (at the expense of higher photon number α^2 to keep the same J). In the numerical simulation, we use J and Δ as independent parameters. Note, however, that the sign of the detuning affects the sign of J. The first dissipative term describes damping (spontaneous and induced emission), and the second dissipative term refers to absorption of thermal fluctuations. The relaxation superoperators are defined by $\mathcal{R}[\hat{b}^\dagger]\hat{A} = \hat{b}^\dagger\hat{A}\hat{b} - \hat{b}^\dagger\hat{b}\hat{A}/2 - \hat{A}\hat{b}^\dagger\hat{b}/2$ (in contrast to the equation for $\hat{\rho}$). For the quadratic Hamiltonian studied here, the equations for the correlators remain closed and are sufficient to describe the Gaussian states produced in the evolution.

We evaluate the logarithmic negativity

$$E_{\mathcal{N}}(\hat{\rho}) = \log_2 \left\| \hat{\rho}_{AB}^{T_A} \right\|_1 \tag{5}$$

as a measure of entanglement for any two given modes (A and B), where $\hat{\rho}_{AB}$ is the state of these two modes, and the partial transpose T_A acts on A only. For Gaussian states, $E_{\mathcal{N}}$ can be calculated via the symplectic eigenvalues of the position–momentum covariance matrix [32].

In figure 3, we show the simulation results for entangling two out of three vibrational modes. The entanglement saturates at later times, while the phonon number grows exponentially. We plot the results at the fixed time $t = 5.6/J$, since there the logarithmic negativity has already saturated. One clearly sees the features predicted above (figure 2), i.e. the unwanted overlap between entanglement processes at higher driving strengths (figures 3(a) and (b)). Increasing the vibrational frequency spacing suppresses these unwanted effects (figure 3(b)). In figure 3(c), the threshold $J = \Gamma\bar{n}$ for entanglement generation at finite temperature is evident, as is the loss of entanglement at large J. Finally, figures 3(d) and (e)

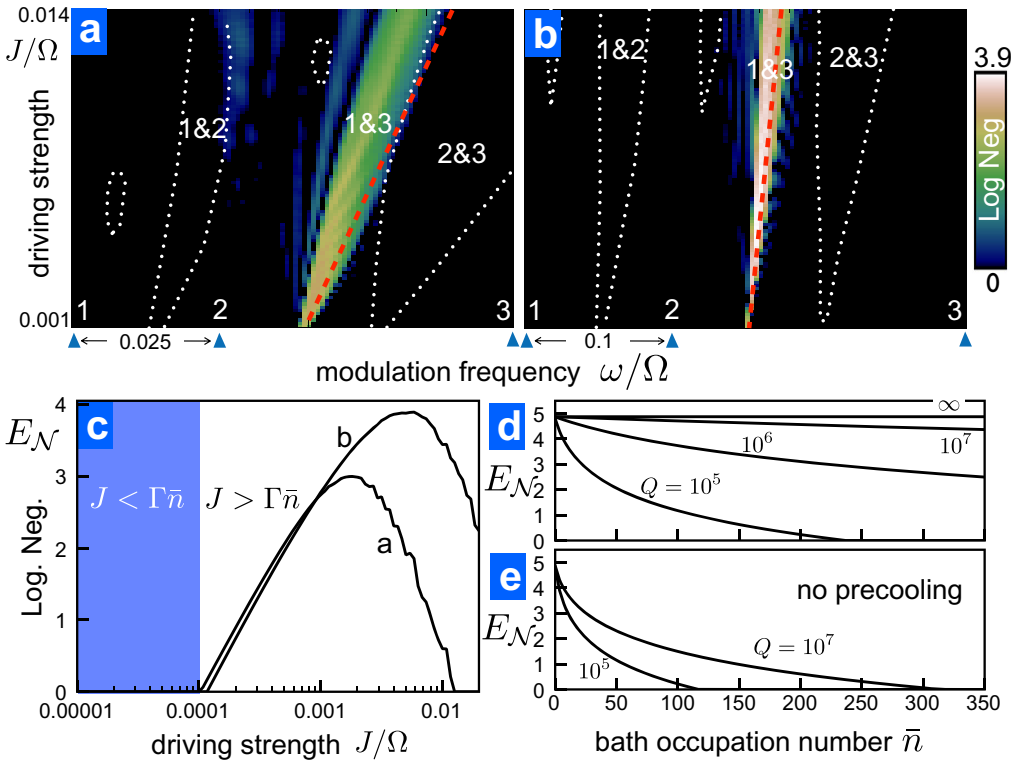

Figure 3. Selective entanglement between two out of three vibrational modes, produced by an amplitude-modulated laser beam driving a common optical mode, as sketched in figure 2. All modes are coupled to a thermal bath and assumed to be cooled to their ground state initially. (a), (b) Entanglement measure (the logarithmic negativity) between modes 1 and 3, as a function of the driving strength J and the modulation frequency ω, at time $t = 5.6/J$. (Contour lines: entanglement between 1 and 2 or 2 and 3 larger than 0.5, blue arrows at Ω_j, red line: resonance position as derived in rotating wave approximation). In (a), the vibrational modes are spaced densely [$\Omega_i = (1, 1.025, 1.075)\Omega$], leading to overlapping resonance regions (as in figure 2). (b) A larger frequency spacing increases the selectivity significantly [$\Omega_i = (1, 1.1, 1.3)\Omega$]. (c) Dependence on driving strength, i.e. cut along dashed red lines in (a) and (b), see the main text. (d) Dependence on temperature and mechanical quality factor Q. (e) The same as (d) but starting from thermal equilibrium. (Parameters: $\bar{n} = 100$, $Q = 10^6$ ((a)–(c)), $\Omega_i = (1, 1.1, 1.3)\Omega$ ((b), (d) and (e)), $J/\Omega = 0.003$ ((d) and (e)), $\Delta = 10\Omega$, $\kappa = \Omega/8$ ((a)–(e)).)

show the dependence on temperature and mechanical quality factor, indicating that this scheme should be feasible for realistic experimental parameters (see below).

3.3. Larger arrays

Having evenly spaced mechanical frequencies is impossible, because the state transfers between adjacent modes would all be addressed at the same modulation frequency. Any simple layout

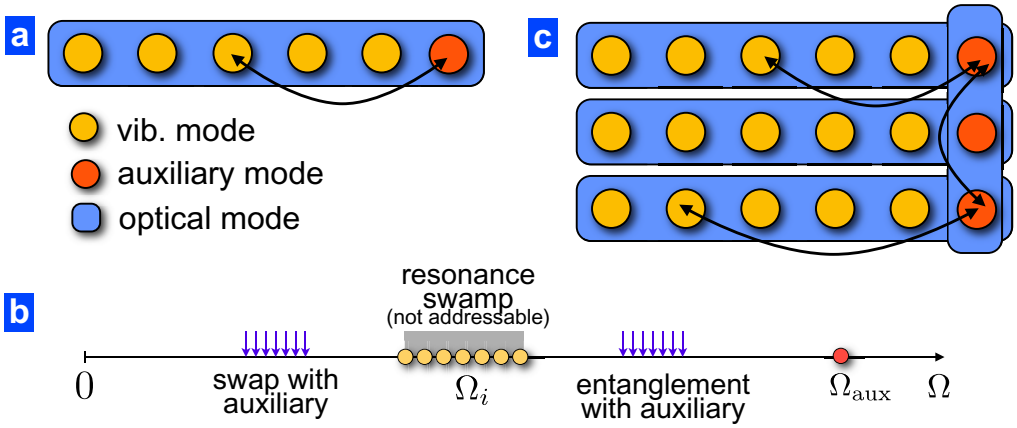

Figure 4. (a) Layout for an optomechanical array with an auxiliary vibrational mode, circumventing the problem of frequency crowding (see the main text). (b) The corresponding mechanical frequency spectrum. The laser modulation frequency has to lie within certain intervals to select entanglement or state-transfer operations between the 'memory modes' and the auxiliary mode (arrows). (c) Extension to a 2D block consisting of three arrays with operations 'around the corner'.

that offers selectivity and avoids resonance overlap seems to require a frequency interval that grows exponentially with the number N of modes. Hence, another approach is needed for large N.

The scheme (figure 4) that solves this challenge involves an auxiliary mode at $\Omega_{\rm aux}$, removed in frequency from the array of evenly spaced 'memory' modes in $[\Omega_{\rm min}, \Omega_{\rm max}]$. All operations will take place between a selected memory mode and the auxiliary mode. Then, the state-transfer resonances are in the band $[(\Omega_{\rm aux} - \Omega_{\rm max})/2, (\Omega_{\rm aux} - \Omega_{\rm min})/2]$, and entanglement is addressed within $[(\Omega_{\rm min} + \Omega_{\rm aux})/2, (\Omega_{\rm max} + \Omega_{\rm aux})/2]$. To make this work, one needs to fulfill the mild constraint $2\Omega_{\rm max} - \Omega_{\rm min} < \Omega_{\rm aux} < 2\Omega_{\rm min}$, where the upper limit prevents unintended driving of the modes caused by the modulated radiation pressure force (see above). Starting with an arbitrary multi-mode state, state transfer between two memory modes is performed in three steps (swapping 1–aux, aux–2 and aux–1), as is entanglement (swap 1–aux, entangle aux–2 and swap aux–1). Note that this overhead does not grow with the number of memory modes. Figure 5 shows the transfer of a squeezed state from the auxiliary mode to a memory mode.

Several such arrays could be connected in a two-dimensional (2D) scheme by linking their auxiliaries with an optical mode (figure 4(c)). The spectrum of the auxiliaries can be chosen as in the introductory example (figure 2), which is allowed by the above constraint and enables selective operations between the auxiliaries. State transfer between memory modes of distinct arrays is possible in five steps (swap $\rm mem_1$–$\rm aux_1$, swap $\rm mem_2$–$\rm aux_2$, swap aux–aux, swap $\rm aux_1$–$\rm mem_1$ and swap $\rm aux_2$–$\rm mem_2$) as well as entanglement (swap $\rm mem_1$–$\rm aux_1$, swap $\rm mem_2$–$\rm aux_2$, entangle aux–aux, swap $\rm aux_1$–$\rm mem_1$ and swap $\rm aux_2$–$\rm mem_2$). Note that the transfer from the memory modes to the auxiliaries can be done in parallel; hence the scheme can be effectively completed in three steps and there is no time delay compared to the single array with auxiliary. Moreover, one might employ more sophisticated transfer schemes [33–35] to improve

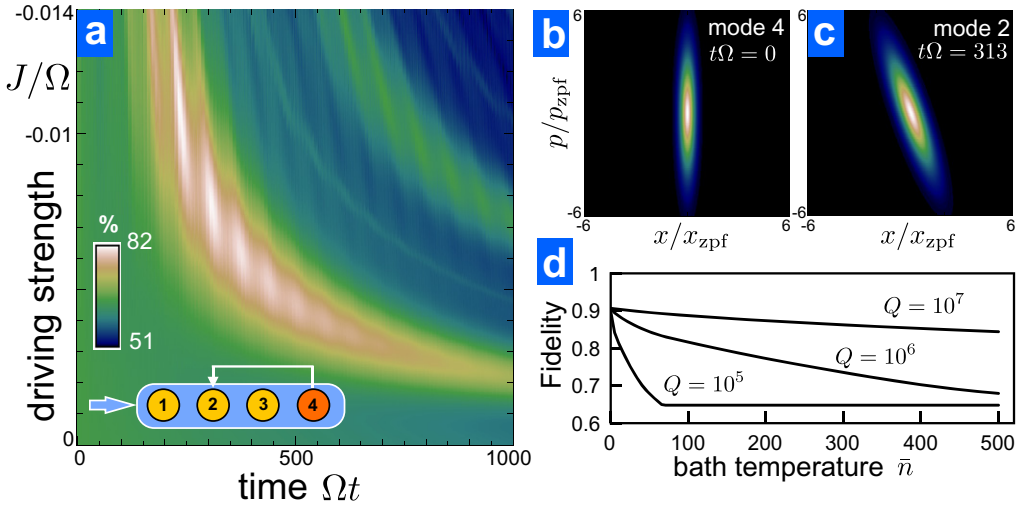

Figure 5. Transfer of a squeezed state ($\Delta x^2 = \mathrm{e}^{-2} x_{\rm ZPF}^2$) from the auxiliary to the second memory mode (all in their ground state due to prior side-band cooling). (a) Dependence of the transfer fidelity on driving strength (negative J due to red detuning $\Delta < 0$) and pulse time (swap pulse ideally at $|J|t = \pi/2$). For long pulse times dissipation hampers the transfer; for large driving strengths resonances overlap, medium times are optimal. (b) The Wigner density of the initial squeezed state in the auxiliary mode and (c) after the transfer. Plotted Wigner density maximizes the transfer fidelity for fixed $J = -0.007\Omega$. (d) Maximization of transfer fidelity over parameter ranges used in (a). (Parameters: $\Omega_j = (1.0, 1.1, 1.2, 1.8)\Omega$, $\bar{n} = 100$, $Q = 10^6$, $\Delta = -20\Omega$, $\kappa = \Omega/8$, $J/\Omega = -0.007$ ((b) and (c)).)

the transfer fidelities. Two blocks can be connected by introducing a higher order auxiliary that couples to both auxiliary arrays. State transfer can then be performed between auxiliary modes from different blocks. In principle, many blocks can be connected when their auxiliary modes are stringed together in a chain via higher order auxiliaries.

4. Implementation

Regarding the experimental implementation, in principle any optomechanical system with long-lived mechanical modes can be used. One promising platform is 'optomechanical crystals' as introduced by Painter and co-workers [4] that feature vibrational defect cavities in the GHz regime with experimentally accessible $Q \sim 10^6$ [36]. These would be very well suited to the scheme presented here, owing to their design flexibility, particularly of 2D structures, and the all-integrated approach, as well as the very large optomechanical coupling strength. Given the currently achieved coupling strength [11, 36] $g_0/2\pi \sim 1\,\mathrm{MHz}$, a detuning of $\Delta/\Omega = 10$ and around 2000 cavity photons (reached in recent experiments), we can estimate the induced coupling to approach the damping rate, $J \sim \Gamma$. This corresponds to the threshold for coherent operations, provided one were to cool down the bath to $k_{\rm B} T_{\rm bath} < \hbar\Omega$. This is, in principle, possible (at 20 mK), but will likely run into practical difficulties due to the re-heating of the structure via spurious photon absorption or other effects. At finite bath temperatures

corresponding to a thermal occupation $\bar{n} \sim k_B T_{bath}/\hbar\Omega$, the light intensity must be increased by a factor of $\bar{n}$ towards $J \gg \Gamma\bar{n}$. Initially, the vibrational ground state would be prepared via laser cooling, as demonstrated in [11].

In these devices, localized vibrational and optical modes can be produced at engineered defects in a periodic array of holes cut into a free-standing substrate. Adjacent optical and vibrational modes are coupled via tunneling. The typical photon tunnel coupling for modes spaced apart by several lattice constants is [6] in the range of several THz. Thus, hybridized optical modes will form, one of which can be selected via the laser driving frequency while the others remain idle. The vibrational modes' frequencies can be different or equal, in which case delocalized hybridized mechanical modes are produced. A 'snowflake' crystal made of connected triangles (honeycomb lattice) supports wave guides (line defects) and localized defect modes with optomechanical interaction [5]. Placing point defects (heavier triangles/thicker bridges) in the structure, a tight binding analysis indicates that the mechanical frequency spectrum (figure 4(b)) can be generated.

Utilizing the phononic modes of an optomechanical system for processing continuous variable quantum information has a number of desirable aspects in comparison to other systems such as optical modes or cold atomic vapors. First, the phononic modes can be integrated on a chip and the devices are thus naturally scalable. The Gaussian operations discussed above can be applied easily, and the decoherence times are already reasonable, although admittedly worse than for cold atomic vapors.

We mention another option for improving the fidelity: optimal control techniques [25] could be employed to numerically optimize the pulse shape $J(t)$.

Finally, an essential ingredient will be the readout. We have pointed out [37] how to produce a quantum-non-demolition readout of the mechanical quadratures in an optomechanical setup. A laser beam (detuning $\Delta = 0$) is amplitude-modulated at the mechanical frequency Ω_j of one of the modes. The reflected light carries information about only one quadrature $e^{i\varphi}\hat{b}_j + e^{-i\varphi}\hat{b}_j^\dagger$. Its phase φ is selected by the phase of the amplitude modulation, while the measurement back-action perturbs solely the other quadrature. Different modes can be read out simultaneously, and the covariance matrix may be thus obtained in repeated experimental runs. Taking measurement statistics for continuously varied quadrature phases would also allow us to perform full quantum-state tomography and thereby ultimately process tomography. Alternatively, short pulses may be used for readout (and manipulation) [38].

5. Conclusions

The scheme described here would enable coherent scalable nanomechanical state processing in optomechanical arrays. It can form the basis for generating arbitrary entangled mechanical Gaussian multi-mode states such as continuous variable cluster states [39]. An interesting application would be to investigate the decoherence of such states due to the correlated quantum noise acting on the nanomechanical modes. Moreover, recent experiments have shown, in principle, how arbitrary states can be written from the light field into the mechanics [7–9]. These could then be manipulated by the interactions described here. Alternatively, for very strong coupling $g_0 > \kappa$, non-Gaussian mechanical states [40–42] could be produced, and the induced nonlinear interactions (see, e.g., [43, 44]) could potentially open the door to universal quantum computation with continuous variables [12] in these systems.

Acknowledgments

We acknowledge the ITN Cavity Quantum Optomechanics, an ERC Starting Grant, the DFG Emmy-Noether program and the DARPA ORCHID for funding.

References

[1] Kippenberg T J and Vahala K J 2008 Cavity optomechanics: back-action at the mesoscale *Science* **321** 1172–6
[2] Favero I and Karrai K 2009 Optomechanics of deformable optical cavities *Nature Photon.* **3** 201
[3] Marquardt F and Girvin S 2009 Optomechanics *Physics* **2** 40
[4] Eichenfield M, Chan J, Camacho R M, Vahala K J and Painter O 2009 Optomechanical crystals *Nature* **462** 78–82
[5] Safavi-Naeini A H and Painter O 2011 Proposal for an optomechanical traveling wave phonon–photon translator *New J. Phys.* **13** 013017
[6] Heinrich G, Ludwig M, Qian J, Kubala B and Marquardt F 2011 Collective dynamics in optomechanical arrays *Phys. Rev. Lett.* **107** 043603
[7] Safavi-Naeini A H, Mayer Alegre T P, Chan J, Eichenfield M, Winger M, Lin Q, Hill J T, Chang D and Painter O 2011 Electromagnetically induced transparency and slow light with optomechanics *Nature* **472** 69
[8] Fiore V, Yang Y, Kuzyk M C, Barbour R, Tian L and Wang H 2011 Storing optical information as a mechanical excitation in a silica optomechanical resonator *Phys. Rev. Lett.* **107** 133601
[9] Verhagen E, Deléglise S, Weis S, Schliesser A and Kippenberg T J 2012 Quantum-coherent coupling of a mechanical oscillator to an optical cavity modes *Nature* **482** 63–7
[10] Teufel J D, Donner T, Dali Li, Harlow J W, Allman M S, Cicak K, Sirois A J, Whittaker J D, Lehnert K W and Simmonds R W 2011 Sideband cooling of micromechanical motion to the quantum ground state *Nature* **475** 359–63
[11] Chan J, Mayer Alegre T P, Safavi-Naeini A H, Hill J T, Krause A, Groeblacher S, Aspelmeyer M and Painter O 2011 Laser cooling of a nanomechanical oscillator into its quantum ground state *Nature* **478** 89
[12] Braunstein S L and van Loock P 2005 Quantum information with continuous variables *Rev. Mod. Phys.* **77** 513–77
[13] Pinard M, Dantan A, Vitali D, Arcizet O, Briant T and Heidmann A 2005 Entangling movable mirrors in a double-cavity system *Europhys. Lett.* **72** 747
[14] Müller-Ebhardt H, Rehbein H, Schnabel R, Danzmann K and Chen Y 2008 Entanglement of macroscopic test masses and the standard quantum limit in laser interferometry *Phys. Rev. Lett.* **100** 013601
[15] Bhattacharya M and Meystre P 2008 Multiple membrane cavity optomechanics *Phys. Rev.* A **78** 041801
[16] Hartmann M J and Plenio M B 2008 Steady state entanglement in the mechanical vibrations of two dielectric membranes *Phys. Rev. Lett.* **101** 200503
[17] Hammerer K, Wallquist M, Genes C, Ludwig M, Marquardt F, Treutlein P, Zoller P, Ye J and Kimble H J 2009 Strong coupling of a mechanical oscillator and a single atom *Phys. Rev. Lett.* **103** 063005
[18] Ludwig M, Hammerer K and Marquardt F 2010 Entanglement of mechanical oscillators coupled to a nonequilibrium environments *Phys. Rev.* A **82** 012333
[19] Akram U and Milburn G J 2012 Photon phonon entanglement in coupled optomechanical arrays *Phys. Rev.* A **86** 042306
[20] Vitali D, Gigan S, Ferreira A, Böhm H R, Tombesi P, Guerreiro A, Vedral V, Zeilinger A and Aspelmeyer M 2007 Optomechanical entanglement between a movable mirror and a cavity field *Phys. Rev. Lett.* **98** 030405
[21] Paternostro M, Vitali D, Gigan S, Kim M S, Brukner C, Eisert J and Aspelmeyer M 2007 Creating and probing multipartite macroscopic entanglement with light *Phys. Rev. Lett.* **99** 250401
[22] Abdi M, Barzanjeh Sh, Tombesi P and Vitali D 2011 Effect of phase noise on the generation of stationary entanglement in cavity optomechanics *Phys. Rev.* A **84** 032325

[23] Tian L, Allman M S and Simmonds R W 2008 Parametric coupling between macroscopic quantum resonators *New J. Phys.* **10** 115001
[24] Serafini A, Retzker A and Plenio M B 2009 Manipulating the quantum information of the radial modes of trapped ions: linear phononics, entanglement generation, quantum state transmission and non-locality tests *New J. Phys.* **11** 023007
[25] Galve F and Lutz E 2009 Energy cost and optimal entanglement production in harmonic chains *Phys. Rev.* A **79** 032327
[26] Bastidas V M, Reina J H, Emary C and Brandes T 2010 Entanglement and parametric resonance in driven quantum systems *Phys. Rev.* A **81** 012316
[27] Galve F, Pachón L A and Zueco D 2010 Bringing entanglement to the high temperature limit *Phys. Rev. Lett.* **105** 180501
[28] Wallquist M, Hammerer K, Zoller P, Genes C, Ludwig M, Marquardt F, Treutlein P, Ye J and Kimble H J 2010 Single-atom cavity qed and optomicromechanics *Phys. Rev.* A **81** 023816
[29] Mari A and Eisert J 2012 Opto- and electro-mechanical entanglement improved by modulation *New J. Phys.* **14** 075014
[30] Mari A and Eisert J 2009 Gently modulating optomechanical systems *Phys. Rev. Lett.* **103** 213603
[31] Marquardt F, Chen J P, Clerk A A and Girvin S M 2007 Quantum theory of cavity-assisted sideband cooling of mechanical motion *Phys. Rev. Lett.* **99** 093902
[32] Vidal G and Werner R F 2002 Computable measure of entanglement *Phys. Rev.* A **65** 032314
[33] Bergmann K, Theuer H and Shore B W 1998 Coherent population transfer among quantum states of atoms and molecules *Rev. Mod. Phys.* **70** 1003–25
[34] Wang Y-D and Clerk A A 2012 Using interference for high fidelity quantum state transfer in optomechanics *Phys. Rev. Lett.* **108** 153603
[35] Tian L 2012 Adiabatic state conversion and pulse transmission in optomechanical systems *Phys. Rev. Lett.* **108** 153604
[36] Chan J, Safavi-Naeini A H, Hill J T, Meenehan S and Painter O 2012 Optimized optomechanical crystal cavity with acoustic radiation shield *Appl. Phys. Lett.* **101** 081115
[37] Clerk A A, Marquardt F and Jacobs K 2008 Back-action evasion and squeezing of a mechanical resonator using a cavity detector *New J. Phys.* **10** 095010
[38] Vanner M R, Pikovski I, Cole G D, Kim M S, Brukner C, Hammerer K, Milburn G J and Aspelmeyer M 2011 Pulsed quantum optomechanics *Proc. Natl Acad. Sci. USA* **108** 16182
[39] van Loock P, Weedbrook C and Gu M 2007 Building gaussian cluster states by linear optics *Phys. Rev.* A **76** 032321
[40] Ludwig M, Kubala B and Marquardt F 2008 The optomechanical instability in the quantum regime *New J. Phys.* **10** 095013
[41] Nunnenkamp A, Børkje K and Girvin S M 2011 Single-photon optomechanics *Phys. Rev. Lett.* **107** 063602
[42] Qian J, Clerk A A, Hammerer K and Marquardt F 2011 Quantum signatures of the optomechanical instability arXiv:1112.6200
[43] Ludwig M, Safavi-Naeini A H, Painter O and Marquardt F 2012 Optomechanical photon detection and enhanced dispersive phonon readout *Phys. Rev. Lett.* **109** 063601
[44] Stannigel K, Komar P, Habraken S J M, Bennett S D, Lukin M D, Zoller P and Rabl P 2012 Optomechanical quantum information processing with photons and phonons *Phys. Rev. Lett.* **109** 013603